TOPICAL REVIEW — Magnetism, magnetic materials, and interdisciplinary research

Recent progress in perpendicularly magnetized Mn-based binary alloy films*

Zhu Li-Jun(朱礼军), Nie Shuai-Hua(聂帅华), and Zhao Jian-Hua(赵建华)†

State Key Laboratory of Superlattices and Microstructures, Institute of Semiconductors, Chinese Academy of Sciences, Beijing 100083, *China*

(Received 2 September 2013)

In this article, we review the recent progress in growth, structural characterizations, magnetic properties, and related spintronic devices of tetragonal Mn_xGa and Mn_xAl thin films with perpendicular magnetic anisotropy. First, we present a brief introduction to the demands for perpendicularly magnetized materials in spintronics, magnetic recording, and permanent magnets applications, and the most promising candidates of tetragonal Mn_xGa and Mn_xAl with strong perpendicular magnetic anisotropy. Then, we focus on the recent progress of perpendicularly magnetized Mn_xGa and Mn_xAl respectively, including their lattice structures, bulk synthesis, epitaxial growth, structural characterizations, magnetic and other spin-dependent properties, and spintronic devices like magnetic tunneling junctions, spin valves, and spin injectors into semiconductors. Finally, we give a summary and a perspective of these perpendicularly magnetized Mn-based binary alloy films for future applications.

Keywords: spintronics, magnetic material, perpendicular magnetic anisotropy, spin polarized transport in semiconductors

PACS: 85.75.–d, 75.50.–y, 75.30.Gw, 72.25.Dc **DOI:** 10.1088/1674-1056/22/11/118505

1. Introduction

Ferromagnetic films with high perpendicular magnetic anisotropy K_u have attracted much attention for their potential applications in nanoscale magnetic devices with high thermal stability.[1–4] Spin valves and magnetic tunneling junctions (MTJs) with high K_u have been demonstrated to allow for the realization of high-sensitivity magnetoresistive sensors, spin-transfer-torque (STT) switching Gbit-class magnetoresistive random access memories (MRAM), and high-power oscillators.[2–5] Magnetic materials that have high K_u, high spin polarization P, high Curie temperature T_c, flexible saturation magnetization M_s, and low magnetic damping constant α are the most ideal candidates for spin-transfer-torque applications, which facilitate reliable switching under a current density below 10^5 A/cm^2.[2–4] Moreover, ferromagnetic films with both high K_u and good compatibility with semiconductors allow not only for the development of ferromagnetic metal/semiconductor hybrid devices including spin field effect transistors,[6,7] spin Hall transistors,[8] spin light emitting diodes,[9,10] and lateral spin valves[12] with perpendicular magnetic anisotropy, but also for the high-density integration of metallic spintronic functional devices like nonvolatile magneto-resistive random access memory on semiconductor photonic and electronic circuits.[12–17] These approaches could also perform logic, communication, and storage within the same material technology taking advantage of nonvolatility, increased integration density, increased speed, and decreased energy consumption compared with the conventional charge-based devices.[18] Furthermore, the demand for high-density data storage leads to the replacement of in-plane magnetic recording by perpendicular magnetic recording. Perpendicular magnetic recording with areal density beyond 10 Tb/inch^2 requires films with high K_u up to 10^7 erg/cc and moderate magnetization M_s.[19] A too high M_s may result in strong coupling between adjacent bits, while a too low M_s brings a low signal–to–noise ratio. Besides, rare-earth magnets provide the backbone of many products including computers, mobile phones, electrombiles, and wind-power generators. However, because of both the increasing limited availability and high costs of mining and processing of rare-earth elements, new kinds of rare-earth-free magnets are urgently needed.[16,20] Permanent magnet applications require materials that have large magnetic energy product, high intrinsic and extrinsic coercivities, and linear demagnetization curves in the second quadruple.

As the most outstanding representatives, perpendicularly magnetized Mn-binary alloys Mn_xGa (MnGa) and Mn_xAl (MnAl) have attracted much attention and been studied intensively in the past couple of decades. $L1_0$-MnGa ($D0_{22}$-Mn_3Ga) alloys are theoretically expected to have K_u of 26 (20) Merg/cc,[21,22] M_s of 845 (305) emu/cc,[16,21–23] $(BH)_{max}=(2\pi M_s)^2$ of 28 (3.7) MGOe,[17,24] P of 71% (88%) at the Fermi level,[17,21,24,25] and α of 0.0003 (0.001).[22] Moreover, $L1_0$-MnAl is theoretically predicted to have K_u of 15 Merg/cc, M_s of 800 emu/cc (or 2.37 μ_B/Mn), and

*Project supported by the National Natural Science Foundation of China (Grant No. 11127406).

†Corresponding author. E-mail: jhzhao@red.semi.ac.cn

© 2013 Chinese Physical Society and IOP Publishing Ltd

$(BH)_{max} = (2\pi M_s)^2$ of 12.64 MGOe.[26,27] These fascinating magnetic properties make MnGa and MnAl promising in spintronics, ultrahigh-density magnetic recording, and economical permanent magnet applications. Moreover, many experimental attempts have been made to the preparations and characterizations of MnGa and MnAl bulks and films, and their related spintronic devices like MTJs, spin valves, and spin-injection devices. In this article, we will present an overview of recent progress on the growth, structural characterizations, magnetic properties, and some other spin-dependent properties of perpendicularly magnetized Mn_xGa and Mn_xAl alloys and their related spintronic devices.

2. Mn_xGa with perpendicular magnetic anisotropy

2.1. Lattice structure and synthesis of Mn_xGa bulks

Alloys of manganese and gallium have a quite complicated phase diagram (Fig. 1(a)) with several magnetically ordered phases.[28–30] This review mainly focuses on the two most interesting tetragonal phases with strong magnetism and high Curie temperature: the first is the $L1_0$-ordered (γ_3) thermal-dynamically ferromagnetic phase at $0.76 \leq x \leq 1.8$;[17,31,32] the second is the $D0_{22}$-ordered (ε) ferrimagnetic phase forming when $2 \leq x < 3$.[25,33–36] The lattice units of both $L1_0$-MnGa and $D0_{22}$-Mn_3Ga are outlined in Fig. 1(b). The lattice unit of $L1_0$-MnGa consists of Mn and Ga monatomic layers stacked alternately along the c axis. The lattice constants of $L1_0$-MnGa bulk (space group $P4/mmm$) are $a = 3.88$–3.90 Å and $c = 3.64$–3.69 Å.[31,32] Bither *et al.* synthesized $L1_0$-Mn_xGa ($1.2 < x \leq 1.5$) polycrystalline bulks.[31] Lu *et al.* systemically investigated the crystalline structure of Mn_xGa bulks in a broad composition range of $1.15 < x < 1.89$.[32] For perfect stoichiometric $L1_0$-MnGa ($x = 1$), each Mn atom is expected to contribute a magnetic moment of $2.51\mu_B$ (corresponding to magnetization of 845 emu/cc); the magnetism of $L1_0$-Mn_xGa may also be strongly influenced by compositions and strains.[16,17,23,25,31,36] As theoretically predicted, excess Mn atoms will align antiparallel to the rest and result in compensation, and strains will also induce a decrease of the Mn magnetic moment.[23,31] For $D0_{22}$-Mn_xGa bulk (space group $I4/mmm$), the lattice constants are $a = 3.90$–3.94 Å and $c = 7.10$–7.17 Å.[33–35] Krén and Kádár obtained $D0_{22}$-$Mn_{2.5}Ga$ bulks by annealing hexagonal $D0_{19}$-Mn_xGa at 350–400 °C for 1–2 weeks, and revealed the ferrimagnetism with Mn atom magnetic moments of $(2.8 \pm 0.3)\mu_B$ and $(1.6 \pm 0.2)\mu_B$ at site I and site II, respectively, by neutron diffraction measurements.[33] Niida *et al.* and Winterlik *et al.* synthesized polycrystalline $D0_{22}$-Mn_xGa bulks in the composition ranges of $1.94 \leq x \leq 2.85$[34] and $2 \leq x \leq 3$,[25] respectively, and revealed the composition-sensitive magnetization in the magnetically frustrated ferrimagnets. With Mn content increasing, lattice constant a slightly increases or keeps the same, while c always decreases monotonically.[25,31–36] Huh *et al.* synthesized Mn_xGa nano-ribbons with $L1_0$ ($x = 1.2$, 1.4, 1.6) and $D0_{22}$ ($x = 1.9$) orderings using arc-melting and melt-spinning followed by a heat treatment and investigated their magnetic and transport behaviors.[37] The Curie temperature of Mn_xGa nano-ribbons is found to increase with increasing x. All the ribbons show a metallic transport behavior in consistent with the Mn_xGa films.

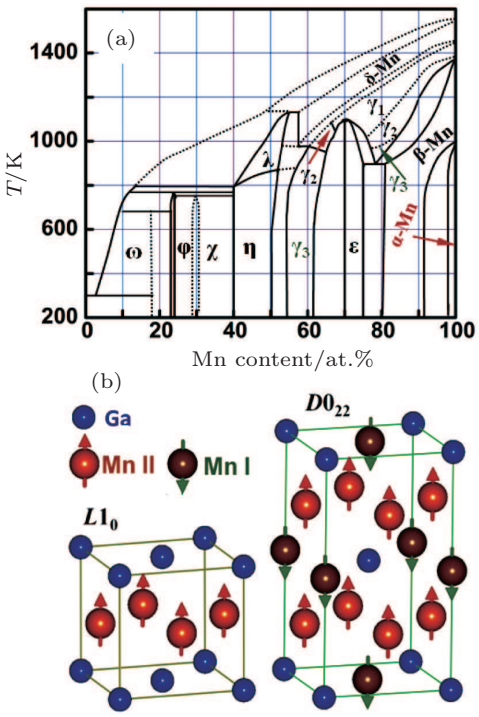


Fig. 1. (a) Phase diagram of Mn–Ga alloys;[30] (b) lattice units of MnGa with $L1_0$ (left) and $D0_{22}$ (right) orderings, arrows give magnetic moment directions of Mn atoms.[17]

The magnetic properties of Mn_xGa alloys, especially giant perpendicular anisotropy, high spin polarization, high Curie temperature, flexible magnetization, and low magnetic damping constant, make this kind of materials promising for applications in magnetic recording, permanent magnets, and spintronic devices like magnetic sensors, memories, and logics.[16,17] Reliable growth of smooth Mn_xGa thin films and effective tailoring of the magnetism are of particular importance for the possible practical applications in not only metal spintronics but also semiconductor spintronics. In the following, we will overview the recent progress in the growth and characterizations of $L1_0$-Mn_xGa films.

2.2. Growth and magnetic properties of Mn_xGa epitaxial films

In the past two decades, a great deal of effort has been made on the growth of $L1_0$- and $D0_{22}$-Mn_xGa films by magnetron sputtering or molecular-beam epitaxy (MBE). Since

Krishnan and Tanaka *et al.* respectively observed the square perpendicular hysteresis of Mn_xGa ($1.2 < x < 1.5$) grown on GaAs (001) by magneto-optical, magnetic, and transportation measurements in the early 1990s,[38,39] the growth and characterizations of $L1_0$-Mn_xGa films have been intensively studied on many kinds of substrates, such as GaN, GaSb, Si, Al_2O_3, and MgO, with different buffer layers (ScN and Cr).[36,40–44] However, only a few of those films on GaAs and MgO demonstrated perpendicular magnetic anisotropy. $D0_{22}$-Mn_xGa films have been prepared mainly on MgO (001) substrates.[22,35,36,45–47] Wu *et al.* reported the magnetic and magneto-transport properties of Mn_xGa ($x = 2.5$, 2.0) epitaxial films on Cr-MgO (001) and even found perpendicular anisotropy in 5 nm-thick films.[45,47] Kurt *et al.* prepared stoichiometric $D0_{22}$-Mn_3Ga films with a perpendicular easy axis on MgO, Pt-MgO, and Cr-MgO, and observed a spin polarization of 58% (40%) in Mn_3Ga (Mn_2Ga).[35,47] Recently, Nummy *et al.* and Zha *et al.* reported nanostructured Mn_xGa films on Si/SiO_2 with coercivity over 20 kOe and discussed the possibility for permanent magnet applications respectively.[48,49] Motivated by the great application potential and inspiring result of Mn_xGa alloys, we prepared Mn_xGa epitaxial films in a wide composition range ($0.76 \leq x \leq 2.60$) on GaAs (001) substrates by MBE, and carried out detailed studies on the tailoring of magnetism in those films with giant perpendicular anisotropy, ultrahigh coercivity, and large magnetic energy product.[16,17]

For practical applications, especially for spintronics, it is essential to choose suitable substrates with small lattice misfit for the epitaxial growth of Mn_xGa films with high magnetic performance, good structural quality, and smooth surfaces. Table 1 summarizes the in-plane lattice constants of representative metals, insulators, and semiconductors with (001) orientation and calculated misfit f of $D0_{22}$-Mn_3Ga ($a = 3.910$ Å) and $L1_0$-MnGa ($a = 3.886$ Å). Simply in view of the lattice misfit, Pt (001), Pd (001), Si (001), $SrTiO_3$ (001), and GaAs (001) should be the best choices for the epitaxial growth of both $D0_{22}$ and $L1_0$ films. To our best knowledge, the report of both $L1_0$- and $D0_{22}$- Mn_xGa epitaxial films grown on Pd is still lacking. Perpendicularly magnetized $L1_0$-Mn_xGa is not available on Si (001) probably due to a strong reaction between the metal layer and the active silicon, though f between $L1_0$-MnGa and Si (001) is only 1.4%.[43] So far, only Pt, GaAs, and $SrTiO_3$ buffers have been experimentally confirmed to be good choices for the epitaxial growth of Mn_xGa films with flat surfaces and high crystalline quality.[16,17,35,47] As a recent review outlined,[24] the surfaces of Mn_xGa films on Cr and MgO buffers appear to be very rough with discontinuous islands,[47] whereas films on Pt and GaAs buffers exhibit very smooth surfaces, since the misfits of $D0_{22}$-Mn_3Ga are –7.2%, –4.0%, –0.3%, and 2.2% for MgO, Cr, Pt, and GaAs buffers, respectively. Therefore, it seems difficult to directly prepare smooth Mn_xGa films on MgO or sharp Mn_xGa-MgO interfaces for high-TMR MTJ due to the large misfit.[50–53] Recently, Glas *et al.* also reported smooth Mn_xGa ($x = 2.9$) films with root mean square (RMS) even below 0.25 nm on $SrTiO_3$.[54] Zhu *et al.* reported Mn_xGa samples ($0.76 \leq x \leq 2.60$) grown on GaAs with good homogeneity and abrupt interfaces[16,17] as revealed by the low-magnification TEM image in the inset of Fig. 2(a).

Table 1. Lattice constants of representative metals, insulators, and semiconductors and calculated misfit in respect to $D0_{22}$-Mn_3Ga (a = 3.910 Å), $L1_0$-MnGa ($a = 3.886$ Å), and $L1_0$-MnAl ($a = 3.920$ Å). The * indicates the lattice constant after 45° in-plane rotation ($a^* = a/\sqrt{2}$).

Buffer	a/Å	$f_{D0_{22}-Mn_3Ga}$/%	f_{L1_0-MnGa}/%	f_{L1_0-MnAl}/%
Cu	3.61	8.3	7.6	8.6
Pd	3.89	0.5	–0.1	0.8
Pt	3.92	–0.3	–0.9	0
Au	4.08	–4.2	–4.8	–3.9
Ag	4.09	–4.4	–5.0	–4.2
Al	4.05	–3.5	–4.0	–3.2
Cr	4.07*	–4.0	–4.6	–3.8
Si	3.94*	–0.8	–1.4	–0.5
$SrTiO_3$	3.91	0	0.8	0.3
GaAs	4.00*	–2.1	–2.7	–1.9
MgO	4.21	–7.2	–7.8	–7.0
InAs	4.28*	–8.6	–9.1	–8.4
AlAs	4.00*	–2.2	–2.7	–1.9

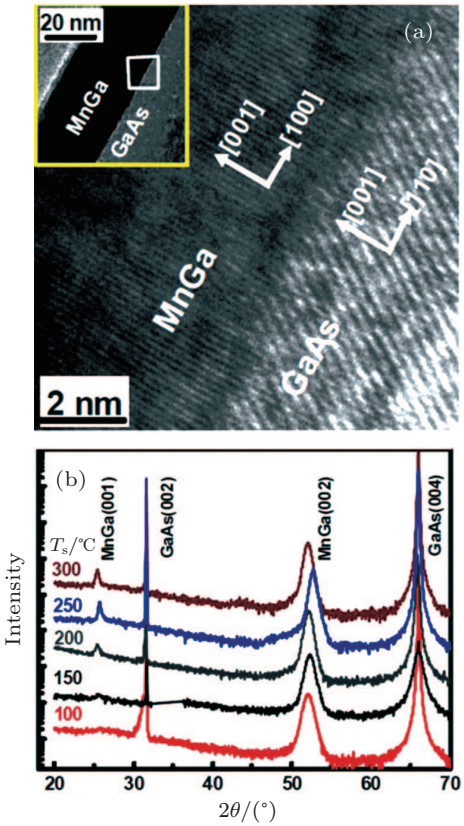


Fig. 2. (a) TEM image of MnGa film ($x = 1.5$) grown on GaAs (001). The inset shows low-magnification TEM image. (b) XRD patterns of MnGa films ($x = 1.5$) grown at 100 °C, 150 °C, 200 °C, 250 °C, and 300 °C, respectively.[16]

The structures and magnetic properties of Mn_xGa films could be tailored effectively by several reliable methods, such as controlling growth temperature T_s,[16] tuning composition x,[17,36] changing annealing conditions,[17] and selecting different substrates.[42,43] In the following, we will show in detail how T_s and x influence the structure and magnetism by taking Mn_xGa films grown on GaAs (001) as examples.

Figure 2(a) representatively shows a high-resolution cross-sectional transmission electron microscopy (TEM) image of Mn_xGa film grown on GaAs,[16] indicating a well-textured Mn_xGa layer with its c axis perpendicular to the GaAs substrate. The epitaxial relationship of MnGa(001)[100]||GaAs(001)[110] can be derived from the high-resolution TEM image, coinciding with the reflection high energy electron diffraction (RHEED) patterns. Figure 2(b) shows examples of synchrotron X-ray diffraction (XRD) θ–2θ patterns of Mn_xGa ($x = 1.5$) films grown at different temperatures.[16] For all the films grown at temperatures between 100 °C and 350 °C, only sharp (001) superlattice peaks and (002) fundamental peaks of $L1_0$-Mn_xGa films can be observed in the range from 20° to 70° besides the peaks of the GaAs substrate, indicating that these are all (001)-textured single-crystalline films with c axis along the normal direction, in agreement with the cross-sectional TEM images and *in situ* RHEED patterns.

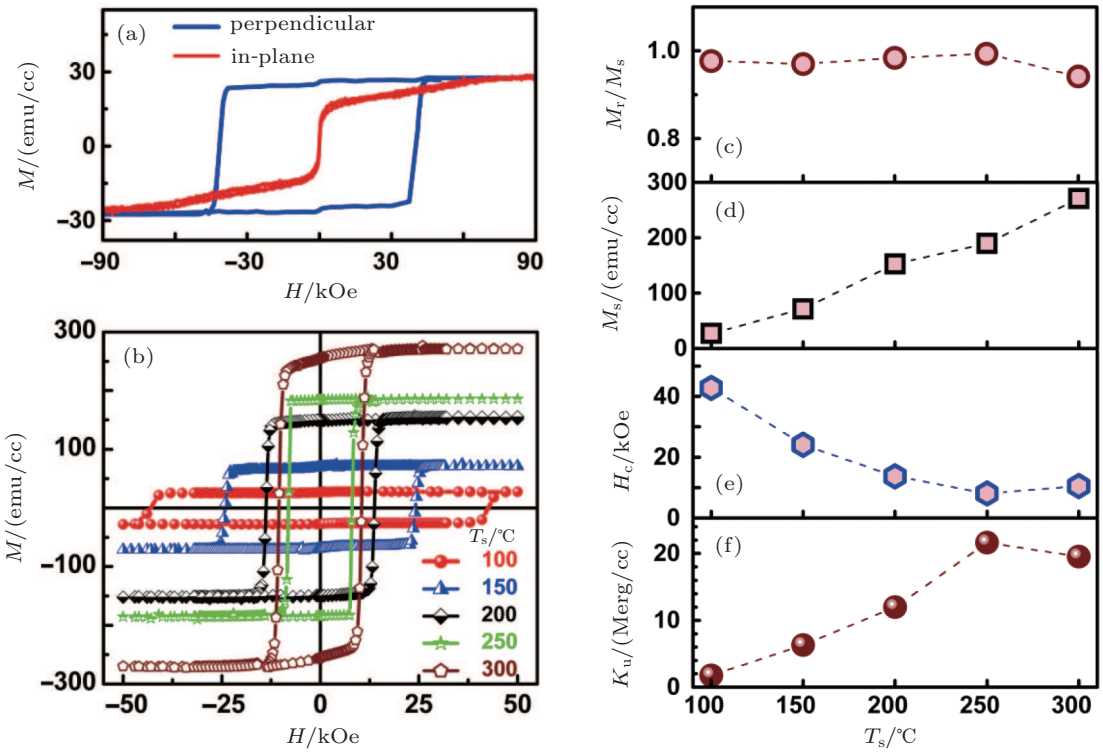


Fig. 3. (a) Perpendicular and in-plane hysteresis loops of the 100 °C-grown $L1_0$-$Mn_{1.5}Ga$ films measured by PPMS. (b) Perpendicular hysteresis loops of the $L1_0$-$Mn_{1.5}Ga$ films grown at different temperatures (T_s) measured by SQUID. (c)M_r/M_s, (d) M_s, (e) H_c, and (f) K_u plotted as a function of T_s.[16]

Figure 3(a) shows both perpendicular and in-plane hysteresis loops of a typical $Mn_{1.5}Ga$ film measured at 300 K.[16] A nearly square loop with ultrahigh coercivity H_c of 42.8 kOe and remnant magnetization M_r of 27.3 emu/cc is observed from the perpendicular M–H curve. However, the in-plane M–H curve exhibits almost an anhysteretic loop, zero remnant magnetization, and high saturation field exceeding 90 kOe. This observation offers a direct evidence for the giant perpendicular magnetic anisotropy. The same feature holds for all the films grown at temperatures between 100 °C and 300 °C. Figure 3(b) shows the perpendicular M–H curves of $Mn_{1.5}Ga$ films grown at different temperatures, revealing a significant influence of growth temperature T_s on the magnetic properties. Figures 3(c)–3(f) summarize the values of M_r/M_s, M_s, H_c, and K_u as a function of T_s. As shown in Fig. 3(c), M_r/M_s keeps a nearly invariant value larger than 0.94 for all the films, very different from those of $L1_0$-$Mn_{1.5}Ga$ films grown on GaN, GaSb, Si, and Al_2O_3.[40–49] The M_s increases monotonically from 27.3 emu/cc to 270.5 emu/cc as T_s increases, which is much smaller than the calculated value of $2.51\mu_B$/Mn ($\sim$ 845 emu/cc) for stoichiometric $L1_0$-MnGa[16,21–23] due to both the overall strains and off-stoichiometry. As shown in Fig. 3(e), H_c has a maximum of 42.8 kOe at 100 °C, then drops to 8.1 kOe at 250 °C, and finally climbs up to 10.8 kOe

at 300 °C. The ultrahigh H_c in these $L1_0$-$Mn_{1.5}Ga$ films is attributed to the combination of giant perpendicular magnetic anisotropy and imperfections including chemical disorder, lattice defects, and overall tensile strains.[16] Importantly, the imperfection contribution to H_c seems to be of the same order of magnitude as the contribution from the magnetic anisotropy since H_c can be tailored so obviously over the large scale from 8.1 kOe to 42.8 kOe. With increasing T_s, K_u goes up monotonically and reaches the maximum value at 250 °C and then decreases with further increasing T_s. The maximum K_u of 21.7 Merg/cc is roughly consistent with the theoretical value of 26 Merg/cc for $L1_0$-$Mn_{50}Ga_{50}$,[21] while much larger than those of Mn_xGa films grown on other semiconductors[38–41] and MgO.[22] Importantly, such a giant K_u of 21.7 Merg/cc in these $L1_0$-$Mn_{1.5}Ga$ films supports nanoscale spintronic devices, such as spin-transfer-torque MRAMs bits, down to 5 nm in size and high-density bit-patterned recording with areal density up to 27 Tb/inch^2 and 60-year thermal stability.[16]

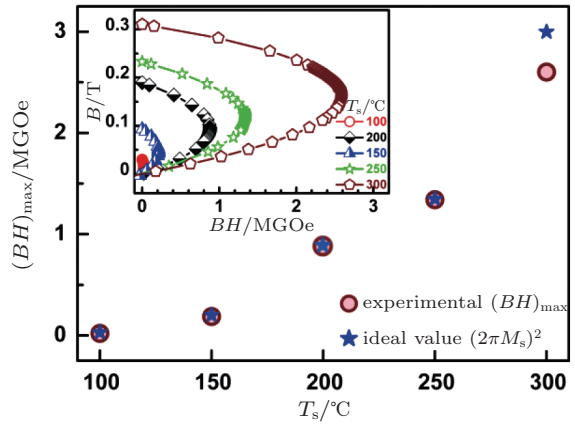


Fig. 4. Comparison of the experimental magnetic energy products $(BH)_{max}$ of $L1_0$-$Mn_{1.5}Ga$ films with ideal value $(2\pi M_s)^2$. The inset shows the *B*–*BH* curves.[16]

Noble-metal-free magnetic materials with a large magnetic energy product are also promising in permanent magnet applications.[20] The magnetic energy product $(BH)_{max}$ of $L1_0$-$Mn_{1.5}Ga$ films is compared with the ideal value $(2\pi M_s)^2$ in Fig. 4. The $(BH)_{max}$ climbs up monotonically from 0.02 MGOe to 2.60 MGOe as T_s increases and is almost the same as the ideal value $(2\pi M_s)^2$ when $T_s < 250$ °C because of the very high M_r/M_s. The $(BH)_{max}$ at $T_s = 300$ °C is slightly smaller than the ideal value probably due to the rounding at the corner of the *M*–*H* loop and the small difference between M_s and M_r ($M_r/M_s = 0.94$). The largest magnetic energy product up to 2.60 MGOe is observed in the film grown at 300 °C, which is larger than that previously reported in bulk polycrystalline $D0_{22}$-$Mn_{2\sim3}Ga$ alloys (< 5.5 kJ/m^3 or 0.68 MGOe)[35] and steel magnets (~ 1 MGOe),[20] and also comparable with hard ferrite magnets (~ 3 MGOe).[20] Therefore, the rare-earth-free composition, high coercivity, and large magnetic energy product together make this kind of $L1_0$-Mn_xGa films promising to be developed for economical permanent magnets.

Both the structure and magnetic properties of Mn_xGa epitaxial films were observed to be very sensitive to the composition. Recently, Mizukami *et al.* and Zhu *et al.* carried out systemic studies on the synthesis and strongly *x*-dependent magnetic properties of (001)-orientated Mn_xGa epitaxial films with $x = 1.2$–3 grown on Cr-buffered MgO (001)[36] and with $x = 0.76$–2.6 grown on GaAs (001),[17] respectively. Figure 5(a) shows examples of XRD θ–2θ patterns of 250 °C-grown Mn_xGa films with different *x* grown on GaAs (001) by MBE.[17] For $0.76 \leq x \leq 1.75$, $L1_0$-MnGa films show both sharp (001) superlattice peaks and (002) fundamental peaks in the range from 20°to 70° besides the peaks of the GaAs substrates, indicating that these are all (001)-textured single-crystalline films. For the film with $x = 0.74$, three small peaks irrelative to $L1_0$ appear, which become dominating for the film with $x = 0.55$. The new phase can be best fitted by cubic $MnGa_4$ with enlarged *c* axis of 3.91 Å. For the film with $x = 2.60$, only the fundamental peak can be found due to the high disorder. As shown in Fig. 5(b), the X-ray reflection (XRR) curves with strong oscillations suggest sharp interfaces and good homogeneity of these samples.

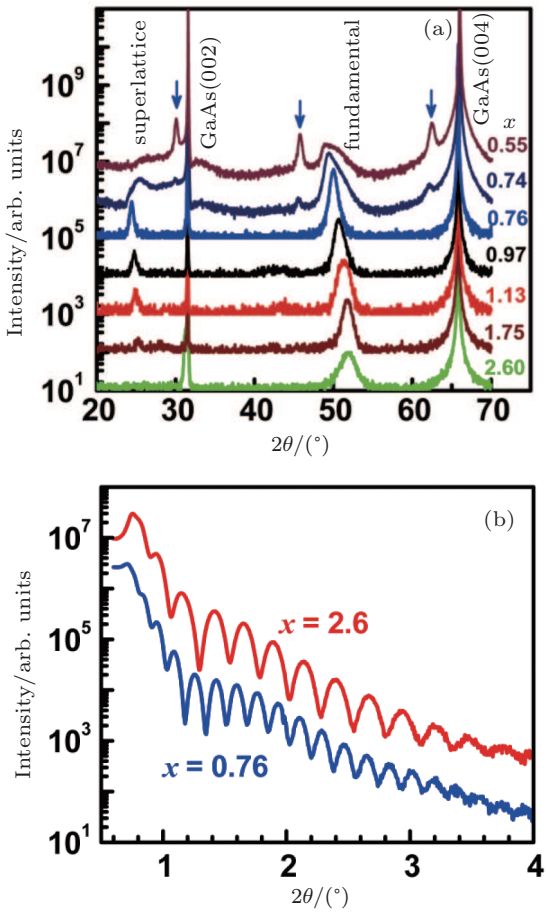


Fig. 5. (a) XRD patterns of MnGa films with different composition *x*. (b) XRR curves of MnGa films with $x = 0.76$, 2.6.[17]

Figure 6(a) shows the typical temperature dependence of

remanent magnetization of Mn_xGa films with a Curie temperature of 630 °C.[17] Figure 6(b) shows an example of hysteresis loops of $L1_0$-$Mn_{1.4}Ga$ films grown at 250 °C.[17] The sample exhibits a fairly square perpendicular loop with high perpendicular coercivity of 11 kOe and anhysteretic in-plane loops with giant saturation fields exceeding 14 T. These characteristics imply strong anisotropy existing in this kind of films.

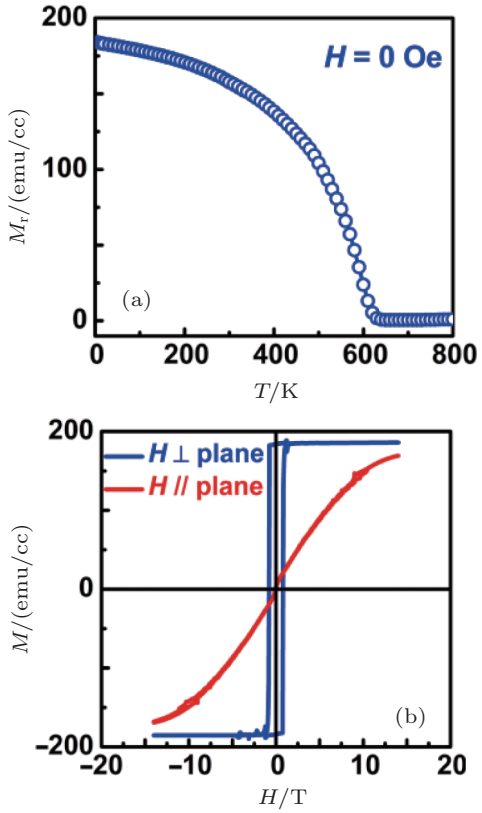


Fig. 6. (a) Temperature dependence of remanent magnetization M_r; (b) perpendicular and in-plane hysteresis loops of $Mn_{1.4}Ga$ film grown at 250 °C.[17]

Figures 7(a)–7(c) display the x-dependent magnetic properties including M_r/M_s, M_s, and H_c determined from the 300 K perpendicular M–H curves of these 250 °C-grown films. The Mn_xGa films with $x = 0.97$–1.75 exhibit high M_r/M_s exceeding 0.90; but those with x out of this range show dramatically decreased M_r/M_s. As shown in Fig. 7(b), M_s decreases dramatically from 450 emu/cc to 52 emu/cc as x increases from 0.76 to 2.60, which should be attributed partly to the increase of antiferromagnetic coupling between Mn atoms at different sites,[21] partly to the increase of strains induced by the short c axis.[16,23] The maximum M_s of 445 emu/cc in $Mn_{0.76}Ga$ is still below the calculated value of 845 emu/cc for stoichiometric $L1_0$-MnGa[16,21] and the experimental value of 600 emu/cc in 400–450 °C-annealed $Mn_{1.17}Ga$ grown on MgO[36] probably due to the low growth temperature. The H_c climbs up from 4.38 kOe to 20.1 kOe as x increases from 0.76 to 1.75, and then drops to 1.1 kOe at $x = 2.60$. This change tendency is consistent well with that of K_u estimated in Fig. 7(d) following the method used in Ref. [16]. The K_u exhibits large values from 8.6 Merg/cc to 21.0 Merg/cc in the $L1_0$ range, while quickly degrades to 0.02 Merg/cc in $D0_{22}$-$Mn_{2.6}Ga$ grown on GaAs because of the increased disorder. Noticeably, $D0_{22}$-Mn_xGa with high ordering and high quality may also demonstrate high K_u values, such as those grown on MgO substrates at high temperatures.[36,45] As ever discussed,[16,25] rare-earth-free and noble-metal-free Mn_xGa alloys are promising for economical permanent magnet applications. Since intrinsic coercivity H_c determined from M–H curves, normal coercivity H_{cB} determined from B–H curves, and magnetic energy products $(BH)_{max}$ are three key features of quality of permanent magnets, we further show H_{cB} and $(BH)_{max}$ in Figs. 7(e) and 7(f). With increasing x in the phase-pure range, both H_{cB} and $(BH)_{max}$ decrease nearly monotonically, corresponding to the decrease of M_s. The film with $x = 1.07$ shows the highest H_{cB} and $(BH)_{max}$ of 3.6 kOe and 3.4 MGOe, respectively. The maximum of 3.4 MGOe is larger than that recent reported in the $Mn_{1.5}Ga$ film (2.6 MGOe)[16] and ferrite magnets (3 MGOe),[20] which makes $L1_0$-Mn_xGa alloys with low Mn compositions still promising to be developed for low-cost and high-performance permanent magnets. Taking into consideration of all the magnetic properties shown in Figs. 7(a)–7(f), low-Mn-composition $L1_0$-Mn_xGa films are more advantageous than the $D0_{22}$ films for applications in magnetic recording with areal density over 10 Tb/inch^2, high-performance nanoscale spintronic devices like MRAM bits with size down to several nanometers, and economical permanent magnet applications, since they simultaneously exhibit high M_r/M_s, M_s, K_u, H_c, H_{cB}, and $(BH)_{max}$.

For further understanding of the composition-dependent magnetism, the structural and magnetic data for typical Mn_xGa films grown on MgO (001) substrates are summarized in Table 2. The magnetization of these films grown on MgO substrates degrades monotonically with increasing x, in consistence with the case of Mn_xGa films grown on GaAs, which should be attributed partly to the increase of antiferromagnetic coupling between Mn atoms at different sites,[21] partly to the increase of strains induced by the short c axis.[16,23] These films also demonstrate giant perpendicular anisotropy K_u of 10^6–10^7 erg/cc and huge coercivity H_c varying from 1 kOe to 18 kOe. Noticeably, H_c always tends to be larger in films with higher Mn composition than that in films with lower Mn composition, while K_u seems to have a complicated dependence on the composition, probably due to the influence of different growth conditions or buffers.

It is also worth mentioning that the magnetism could be effectively tailored by post-growth annealing[17] and choosing different substrates. By using different substrates like semiconductors (GaAs, GaSb, GaN, Si, ScN, etc), insulators (SiO_2, Al_2O_3, MgO, etc), and metals (Cr, Pt, etc), Mn_xGa films

could crystallized into different structures, such as different crystalline orientations,[42,43] different morphologies,[35,47–49] and different strains,[16] and further have different magnetic anisotropies and other magnetic properties. Therefore, Mn_xGa films are observed to exhibit giant perpendicular magnetic anisotropy, flexible magnetization, huge coercivity, large energy product, and high Curie temperature. Meanwhile, the magnetism of Mn_xGa films could be effectively tailored via several reliable ways, especially by controlling the growth temperature, tuning the composition, post-growth annealing, and selecting substrates. These data provide a comprehensive diagram for tailoring and improving the structure and magnetism of Mn_xGa films, which would be helpful for understanding this kind of material and approaching successful applications in various spintronic devices, magnetic recording, and permanent magnets.

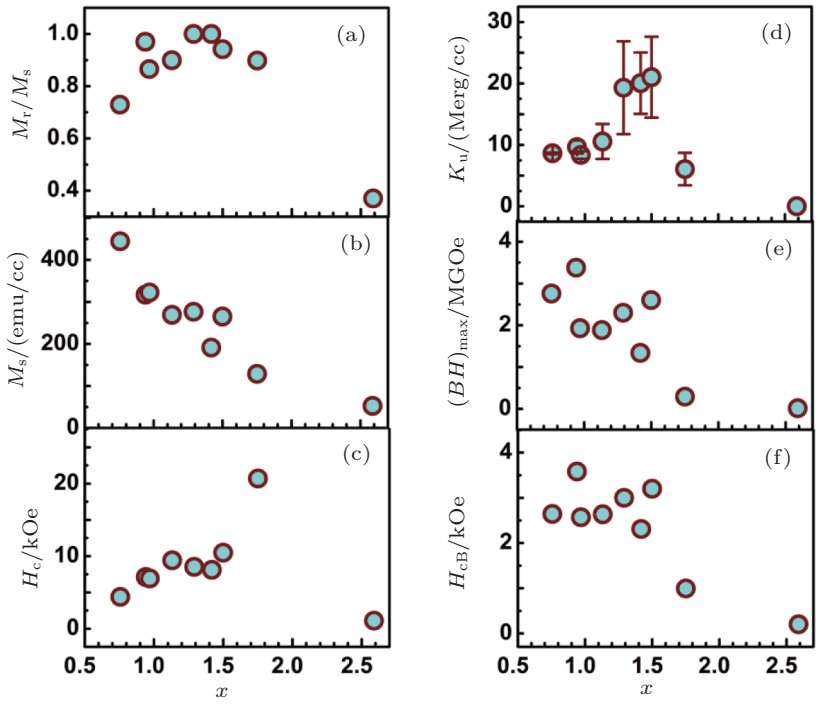


Fig. 7. Composition x dependences of (a) M_r/M_s, (b) M_s, (c) H_c, and (d) K_u of Mn_xGa films grown on GaAs (001) at 250 °C.[17]

Table 2. Structural parameters and magnetic data of typical Mn_xGa films grown on MgO (001), T represents the growth or annealing temperature.

	Substrate	T/°C	a/Å	c/Å	M_s(300 K)/(emu/cc)	K_u(300 K)/(Merg/cc)	H_c(300 K)/kOe	Reference
Mn_3Ga	Pt-MgO	250	–	7.12	110	8.9	18	[35], [47]
Mn_3Ga	MgO	350	–	7.07	140	19.1	18	[35], [47]
Mn_3Ga	Cr-MgO	350	–	6.96	140	4	17	[35], [47]
Mn_3Ga	Cr-MgO	400	–	7.10	200	–	15	[36]
$Mn_{2.5}Ga$	Cr-MgO	400	3.91	7.11	250	12	6	[46]
$Mn_{2.1}Ga$	MgO	450–500	3.92	7.11	305	15	–	[22]
Mn_2Ga	MgO	360	–	7.16	470	23.5	3.6	[35]
$Mn_{1.2}Ga$	Cr-MgO	400–500	3.90	3.60	600	15	1	[36]

2.3. Other spin-dependent properties of Mn_xGa epitaxial films

2.3.1. Spin polarization

For magnetic sensors, memories, and oscillators, it is advantageous to use materials with high spin polarization, which allows for high magnetoresistance ratios and high signal to noise ratios. As calculated by Sakuma and Winterlik *et al.,* stoichiometric $L1_0$-MnGa and $D0_{22}$-Mn_3Ga should have high spin polarization of 71% and 88% at the Fermi level, respectively.[21,25] The spin polarization is also predicted to decrease with increasing Mn deficiency, atomic disorder, and strain.[25] Kurt *et al.* performed point contact Andreev reflection spectroscopy measurements and determined spin polarization of 58% and 40% at 2.2 K in $D0_{22}$-Mn_3Ga and Mn_2Ga films, respectively.[47] Higher spin polarization is expected in perfectly ordered $D0_{22}$-Mn_xGa films although detailed investigations are still absent. To our best knowledge, there have

also been no available reports about the experimental measurements of spin polarization of $L1_0$-Mn_xGa alloys. Further investigations on spin polarization are needed.

2.3.2. Magnetic damping

Spin-transfer-torque (STT) is a phenomenon of magnetization switching induced by a spin current. For STT-driven spintronic devices, a low critical current for current-induced magnetization switching is preferred for low energy consumption and reliable switching.[2,55] The critical switching current can be written as

$$I_{c0}=\alpha K_u V \frac{\gamma e}{\mu_B g(P,\theta)}, \quad (1)$$

where α is the magnetic damping constant; K_u is the perpendicular anisotropy; V is the volume of magnets; γ is the gyromagnetic ratio; μ_B is the Bohr magnetron; e is the the elementary charge; and $g(P,\theta)$ is a function of the spin polarization (P) of the tunnel current and the angle (θ) between the magnetization of the free and the reference layers.

As indicated in Eq. (1), perpendicular magnetized materials with combination of high P, low α, and low K_u are preferred for low-switching-current STT device applications. Generally, a high K_u and a low critical switching current I_{c0} are in contrast, but a high K_u is absolutely essential for long time stability. However a combination of high P and K_u with low enough α could still provide a possibility for a low I_{c0} and long time thermal stability. Except for the high P and K_u, the noble-metal-free Mn_xGa alloys also have much lower magnetic damping constants than those of all the other perpendicular-anisotropy materials to our best knowledge due to the low density of states at the Fermi level and the weak spin–orbit interaction in light 3d elements Mn and Ga.[22] Time-resolved MOKE experiments revealed the damping constant of 0.008 (0.015) for $Mn_{1.54}Ga$ ($Mn_{2.12}Ga$) films, which is one or two order smaller than that of known materials with large perpendicular anisotropy.[2] First-principles calculations indicated an even lower damping constant of 0.0003 (0.001) for $L1_0$-MnGa ($D0_{22}$-Mn_3Ga) defect-free alloys.[22] Therefore, with respect to both high thermal stability and low critical switching current, Mn_xGa alloys with either $L1_0$ or $D0_{22}$ ordering are advantageous for low-current-switching STT-memory and oscillator applications.

2.3.3. Magneto-optical Kerr effect

Perpendicularly magnetized materials with large Kerr rotation angle and optical reflectivity are also promising in high-density perpendicular magneto-optical recording. Krishnan first studied the magneto-optical properties of $L1_0$-$Mn_{1.5}Ga$ films grown on GaAs (001) in 1992.[38] The film exhibited a large Kerr rotation angle of $\sim 0.1^\circ$ at 820 nm. Furthermore, reflectivity around 65%–70% was found over a broad wavelength range from ultraviolet to far infrared. From a technological point of view, the epitaxial growth on semiconductor and the high-performance magneto-optical properties would make the exciting possibility of the integration of magneto-optic and semiconductor devices a reality.

2.3.4. Anomalous Hall effect

The anomalous Hall effect (AHE), related to the spin–orbit interaction in magnetic materials, has potential for sensor, memory, and magnetic logic applications.[45] A large AHE has been observed in various perpendicularly magnetized films including $L1_0$-FePt, FePd, etc.[56,57] Accordingly, the study of AHE in Mn_xGa films is of great importance not only for practical applications but also for comprehending the widely disputed mechanism of AHE. Tanaka *et al.* measured the AHE hysteresis of $L1_0$-$Mn_{1.5}Ga$ films on GaAs and found the sample-dependent AHE resistivity, changing from 0.5 μΩ·cm to 4 μΩ·cm.[39] Bedoya-Pinto revealed a noticeably composition-dependent scaling behavior in $L1_0$-Mn_xGa ($x = 0.96$, 1.38, 2.03) films on GaN.[41] Wu *et al.* observed AHE resistivity up to 11.5 μΩ·cm in $D0_{22}$-Mn_2Ga,[45] which is much larger than that of other perpendicular-anisotropy materials, such as $L1_0$-FePt (1–6 μΩ·cm).[56,57] Glas *et al.* studied $D0_{22}$-Mn_xGa ($x = 2.3$, 2.6, 2.9) films grown on MgO and $SrTiO_3$, and discussed the determined skew scattering and side jump coefficients with regard to the film composition and compared to the crystallographic and magnetic properties.[54] Zhu *et al.* reported AHE and the scaling behavior of $L1_0$-$Mn_{1.5}Ga$ films grown on GaAs (001) and found the significant influence of disorder on the scaling behavior.[58] However, for further understanding of the underlying physics, more detailed studies will be needed.

2.4. Thermal and chemical stability

The structural stability of materials is of particular importance for practical applications. $L1_0$-ordered Mn_xGa have been widely believed to keep thermal-dynamically stable up to at least 800 K,[31,32] in contrast, Mn_xGa with $D0_{22}$ ordering are observed to be metastable and will transfer to antiferromagnetic hexagonal $D0_{19}$ phase at temperature over 770 K.[25,33,34] Zhu *et al.* investigated the thermal stability of the MnGa/GaAs interface by performing systematical post-growth annealing experiments taking the $L1_0$-$Mn_{0.76}Ga$ film as an example, which exhibits the largest M_s among all the as-grown films with different x (Fig. 7(b)). Figure 8(a) shows XRD patterns of as-grown and 10 min-annealed $Mn_{0.76}Ga$ films, from which we find that the $Mn_{0.76}Ga$ film itself is thermal stable up to 450 °C, and the interface could keep stable up to at least 350 °C. These results roughly agree with the previous report that Mn_xGa with $x < 1.5$ should keep stable on GaAs below 400 °C.[59] Interestingly, a very weak

Mn_2As (003) peak as a result of the interfacial reaction is observable in high-sensitivity synchrotron XRD measurement, which may be undetectable by the common XRD with Cu $K\alpha$ radiation.[59] Fortunately, the stable temperature of at least 350 °C could still satisfy the demand of integration with metal-oxide-semiconductor transistors.

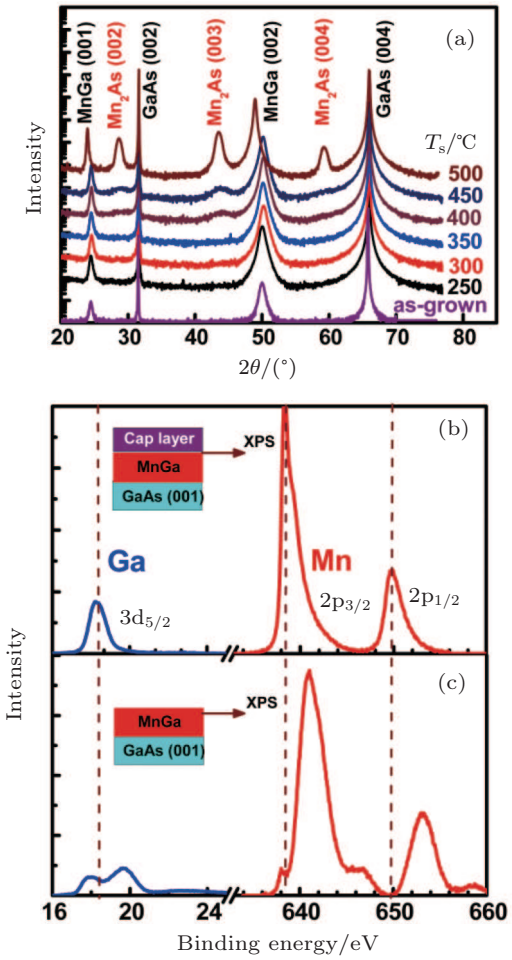


Fig. 8. (a) XRD patterns of $Mn_{0.76}Ga$ films annealed at 250 °C, 300 °C, 350 °C, 400 °C, and 450 °C, respectively;[17] XPS patterns of $Mn_{0.97}Ga$ films (b) with and (c) without an Al cap layer after exposure in air atmosphere for a week.[24]

There have been disputes on the chemical stability of Mn_xGa alloys in the ambient conditions. Roy *et al.* found an oxide layer of less than 5 nm formed at the Mn_xGa surface,[60] however Wang *et al.* found no signs of oxidation of Mn_xGa films in air atmosphere.[61] In fact, a capping layer is always used to prevent the possible oxidation of Mn_xGa films.[16,36,38] In order to make clear the chemical stability in the ambient conditions, we show in Fig. 8(b) X-ray photoelectron spectroscopy (XPS) of Mn and Ga on the surfaces of Mn_xGa films with and without the capping layer which have been exposed in the air at room temperature for a week.[24] Mn_xGa films with Al capping layer show asymmetric elemental peaks in both Mn 2p and Ga 3d spectra. The asymmetry of these peaks should be attributed to the significant shielding effect to the core levels by the high density at the Fermi level due to the alloy nature of the film, which further reveals the good protection of a 2 nm Al layer from oxidation. By contrast, Mn_xGa films without Al capping layer show evident peak shifts and reduced asymmetry, indicating significant oxidation occurred. Therefore, it is necessary to protect Mn_xGa films from oxidation by using suitable capping layers.

2.5. Mn_xGa-based spintronic devices

Magnetic tunneling junctions and giant magnetoresistance (GMR) devices based on perpendicularly magnetized materials are expected to ensure the thermal stability of nanoscale spintronic devices and to be developed as high-performance MR sensors, STT-MRAM, and STT oscillators. As discussed above, (001)-orientated Mn_xGa alloys with $L1_0$ or $D0_{22}$ ordering simultaneously show giant K_u, high P, high T_c, huge H_c, moderate M_s, and low α, which make this kind of materials an ideal combination for high-field sensors, Gbit STT-MRAM, and high-power STT oscillators. Recently, a few groups have carried out theoretical and experimental work from this point of view. Using first-principles calculations based on the density functional theory and non-equilibrium Green's function, Bai *et al.* predicted large tunnel magnetoresistance (TMR) effect of 1000% in Mn_2Ga/MgO/Mn_2Ga MTJs, whereas no tunneling magnetoresistance effect in the Mn_3Ga/MgO/Mn_3Ga MTJ stack due to the symmetry selective spin filtering effect of MgO.[62] Kubota *et al.* observed TMR ratios no more than 23% at 10 K and annealing endurance up to 375 °C in a series of Mn_xGa/MgO/CoFe MTJs with different compositions of the Mn_xGa electrode.[50] The small TMR ratios were attributed to the large misfit between MgO and Mn_xGa, which may cause lattice dislocations and an unfavorable growth of the MgO barrier. Kubota *et al.* further made attempts to improve the TMR ratios by using Fe or Mg insertion layers at the Mn_xGa and MgO interface,[51,52] however, the optimized TMR ratios were still below 25% at 10 K. So far, the highest TMR ratio in Mn_xGa-based MTJs is 40% at room temperature observed in the $Mn_{1.63}Ga$/MgO/CoFeB MTJ with Co (1.5 nm)/Mg (0.4 nm) insertion between $Mn_{1.63}Ga$ and MgO.[53] Noticeably, Zha *et al.* also fabricated a (112)-textured $Mn_{2.3-2.4}Ga$/Cu/CoFe current-in-plane pseudo spin valve with GMR up to 3.88%.[63] Roy *et al.* studied the oscillatory dependence of the interlayer exchange coupling strength on the spacer layer thickness in Mn_xGa/GaAs (Mn_2As, Mn_2Sb)/Mn_xGa trilayers.[64] In addition, Adelmann *et al.* demonstrated the electrical spin injection from $Mn_{1.38}Ga$ into (Al,Ga)As p–i–n light-emitting diode (LED) at remanence.[12]

It is still an exciting field to explore Mn_xGa-based MTJs, spin valve devices, and semiconductor spintronic devices with high performance for practical applications, and to take advantage of the amazing properties of this candidate material.

3. $L1_0$-Mn_xAl epitaxial films on semiconductors

3.1. Lattice structures and syntheses of Mn_xAl bulks

Despite the complex phase diagram (Fig. 9),[65] alloys of Mn and Al only have one ferromagnetic phase with a lattice unit similar to that of $L1_0$-MnGa (i.e., τ-phase) shown in Fig. 1(b). The lattice constants of the $L1_0$-MnAl bulk are $a = 3.92$ Å and $c = 3.57$ Å.[66] In 1960, Koch *et al.* synthesized $L1_0$-$Mn_{1.25}Al$ bulk by rapid cooling of nonmagnetic ε-MnAl and observed T_c of 653 K, M_s of 490 emu/cc, K_u of ~ 10 Merg/cc, and $(BH)_{max}$ of 3.5 MGOe.[66] In 1977, Ohtani *et al.* synthesized an MnAl bulk with a giant $(BH)_{max}$ over 7 MGOe by doping C element into the alloy.[67] As shown in Fig. 9, a composition range with x from 1 to 1.5 and an annealing temperature between 500 °C to 900 °C are needed for the syntheses of $L1_0$-MnAl bulks. $L1_0$-MnAl bulks are in the metastable phase and easily decompose into β-Mn and nonmagnetic γ-MnAl.

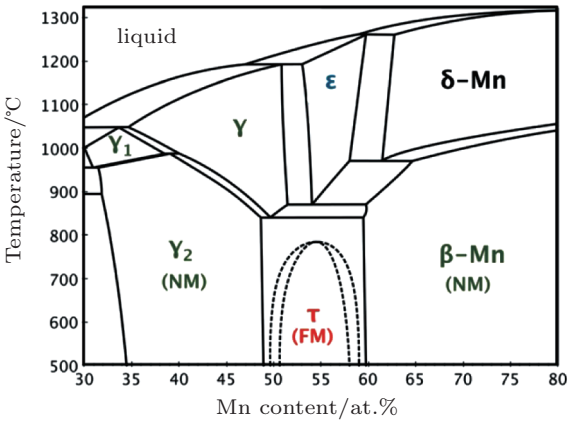


Fig. 9. Binary phase diagram of MnAl alloys.[65]

3.2. Growth and magnetic properties of Mn_xAl epitaxial films

Since 1990s, the growth and magnetic properties of $L1_0$-MnAl thin films have been widely studied on AlAs-buffered GaAs (001),[68,69,71–74] GaAs (001),[26,70] Cr-buffered MgO (001),[75,76] and glass[77] by MBE, sputtering, e-beam evaporation, and pulse laser deposition. Despite those progresses, only a few $L1_0$-MnAl epitaxial films grown on GaAs (001) and MgO (001) substrates exhibited perpendicular magnetic anisotropy.[68–76] We should point out that many metal (e.g., Pt, Pd, Al, Cr, etc), insulator, (e.g., $SrTiO_3$), and semiconductor (e.g., Si, GaAs, InAs, AlAs) buffers could allow the epitaxial growth of $L1_0$-MnAl thin films in view of the lattice mismatch (Table 1). However, there are no available reports on the epitaxial growth of $L1_0$-MnAl thin films on buffers or substrates other than GaAs (with or without AlAs buffer) and Cr-buffered MgO (001).

The magnetic properties of $L1_0$-MnAl thin films are observed to be very sensitive to the composition and growth temperature. As investigated recently,[70] although $L1_0$-ordered Mn_xAl films could have been epitaxially grown on GaAs (001) in a wide composition range with x from 0.5 to 1.2, films with $x = 1.1$ exhibit the strongest XRD satellite peaks, indicating the optimized composition and the nearly perfect $L1_0$-ordered superlattice structures. $Mn_{1.1}Al$ (or $MnAl_{0.9}$) also shows the highest M_r/M_s and M_s.[70] For further optimizing and tailoring of the structure and magnetic properties, systematical experiments were carried out on the growth temperature effects.[26] As shown in Fig. 10, the XRD patterns for $Mn_{1.1}Al$ films grown at different T_s from 100 °C to 400 °C reveal that all the $Mn_{1.1}Al$ films are single-crystalline with c axis along the normal direction. Moreover, the $Mn_{1.1}Al$ film grown at 350 °C exhibits satellite peaks disclosing the optimized growth temperature range for the best crystalline quality. However, $Mn_{1.1}Al$ films grown beyond 250 °C show a peak of nonmagnetic ε phase. The sharp interface between $Mn_{1.1}Al$ and GaAs is confirmed by both the high-resolution TEM image and XRR curves.

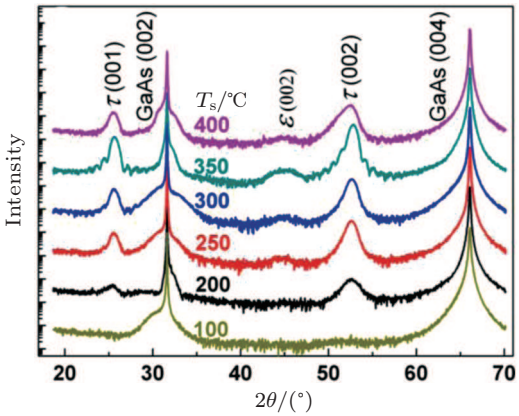


Fig. 10. XRD patterns of $L1_0$-$Mn_{1.1}Al$ films grown at 100 °C, 200 °C, 250 °C, 300 °C, 350 °C, and 400 °C, respectively.[26]

Figure 11(a) shows the typical perpendicular and in-plane hysteresis loops of $L1_0$-$Mn_{1.1}Al$ sample grown at 350 °C. The almost square perpendicular hysteresis loop and anhysteretic in-plane hysteresis loop clearly demonstrate that the sample is more easily magnetized in the out-of-plane direction. The perpendicular hysteresis loops of MnAl films grown at different T_s are shown in Fig. 11(b), and it can be found that perpendicular M_r/M_s, M_s, H_c, and K_u strongly depend on T_s, the details of which are summarized in Figs. 11(c) and 11(d). The M_s increases from 47.8 emu/cc to 361.4 emu/cc as T_s increases from 100 °C to 350 °C, and then decreases to 316.4 emu/cc at 400 °C. These changes are mainly linked to the crystalline quality of the samples. The H_c has a minimum of 330 Oe at 100 °C, then increases to 10.7 kOe at 250 °C, and finally drops to 8.1 kOe at 400 °C. The K_u shows a maximum of 15 Merg/cc

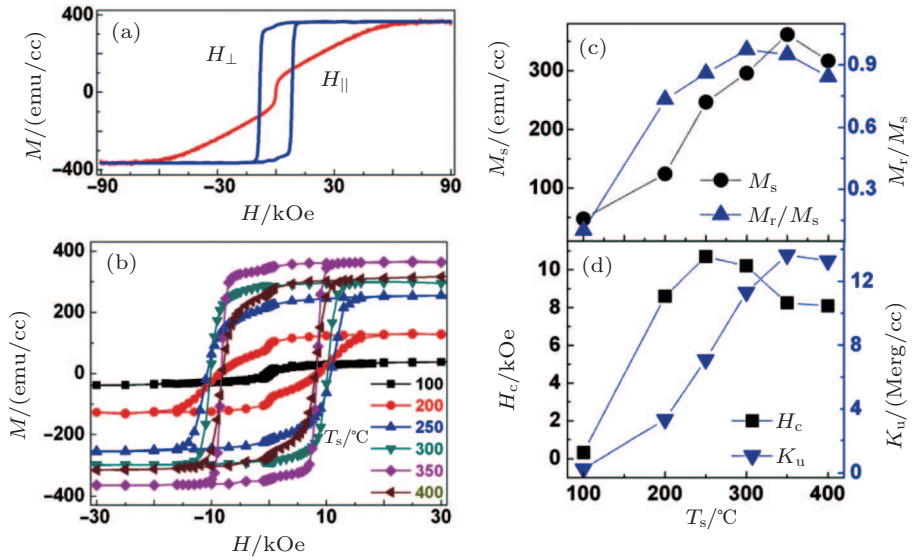


Fig. 11. (a) Perpendicular and in-plane hysteresis loops of the 350 °C-grown $L1_0$-$Mn_{1.1}Al$ films. (b) Perpendicular hysteresis loops of the $L1_0$-$Mn_{1.1}Al$ films grown at different temperature T_s. (c) M_r/M_s, M_s, (d) H_c and K_u plotted as a function of T_s.[26]

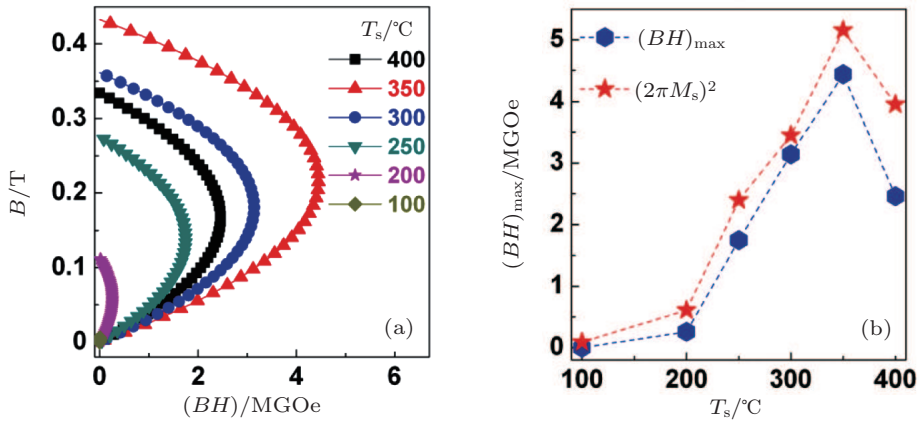


Fig. 12. (a) The T_s dependence of the magnetic energy products. (b) Comparison of the experimental $(BH)_{\max}$ with ideal value $(2\pi M_s)^2$.[26]

Table 3. Structure parameters and magnetic data for representative Mn_xAl films grown on different substrates, $T_s(T_a)$ represents the growth (annealing) temperature.

	Substrate	$T_s(T_a)$ /°C	a/Å	c/Å	M_s(300 K)/(emu/cc)	K_u(300 K)/(Merg/cc)	H_c(300 K)/kOe	Reference
$Mn_{1.50}Al$	AlAs-GaAs	200–270 (350)	–	3.41	285	–	~4.0	[73]
$Mn_{1.11}Ga$	GaAs	350	–	3.47	361	13.7	~8.0	[26]
$Mn_{1.32}Al$	Cr-MgO	250 (250)	–	~3.57	530	10	–	[75]
$Mn_{0.92}$ Al	Cr-MgO	200 (450)	3.92	3.57	600	10	–	[76]

at 350 °C. Moreover, MnAl films are another candidate for rare-earth-free permanent magnets. As shown in Fig. 12(a), $(BH)_{\max}$ first increases from 0.001 MGOe to 4.44 MGOe as T_s increases from 100 °C to 350 °C, then decreases to 2.46 MGOe at 400 °C. As compared in Fig. 12(b), the experimental value of $(BH)_{\max}$ is lower than the ideal value $(2\pi M_s)^2$ probably due to the differences between M_s and M_r and the rounding of the M–H loops. The largest $(BH)_{\max}$ up to 4.44 MGOe is larger than that of previously reported in MnAl alloys (3.5 MGOe),[66] $Mn_{1.5}Ga$ films (2.6 MGOe),[16] and hard ferrite magnets (3 MGOe).[20]

For better understanding, the typical data of structures and magnetic properties of MnAl films grown on different buffers are compared in Table 3. Mn_xAl films grown on AlAs and GaAs buffers exhibite much lower magnetization than bulk and films grown on Cr-MgO, which is probably related to the shorter c axis and the corresponding strains. Noticeably, despite the different buffers and different growth (annealing) temperature, most MnAl films display a high K_u exceeding 10 Merg/cc. Here, we need to mention that there have been no detailed studies on the growth of smooth MnAl films on MgO and $MgAl_2O_4$,[78] which is essential for the development of

MnAl-based MTJs and spin-injection devices with a MgO or $MgAl_2O_4$ barrier.

3.3. Other spin-dependent properties

3.3.1. Magneto-optical Kerr effect

Cheeks *et al.* investigated the polar magneto-optical Kerr effect in 5-nm and 10-nm thick $L1_0$-MnAl epitaxial films grown on AlAs-buffered GaAs (001) and found a large Kerr rotation of 0.11° in a wide wave length range from 220 nm to 820 nm.[71] The value 0.11° is modest compared to 0.3°–0.4° reported for materials such as TbFeCo currently used in the industry. Although thicker films are expected to give a higher Kerr rotation, there is so far no further progress report available.

3.3.2. Anomalous Hall effect

The anomalous Hall effect of $L1_0$-MnAl films was intensively studied in 1990s. Sands *et al.*[68] and Leadbeater *et al.*[69] prepared single-crystalline $L1_0$-MnAl films on AlAs-GaAs (001) with perpendicular *c* axis and observed large Hall hystereses. Angadi and Thanigaimani reported the Hall effect of MnAl films evaporated on glass substrates with different compositions and different thicknesses (25–150 nm), and found that the ordinary Hall coefficient R_0 and anomalous Hall coefficient R_s are of the same order over the entire thickness range.[77] Both R_0 and R_s are positive for thinner layers, and negative for thicker ones. Boeck *et al.* observed rectangular Hall hysteresis loops in $Mn_{1.5}Al$ grown on AlAs-GaAs (001) and AHE resistivity in the order of 4–8 μΩ·cm,[72] depending on the width of the Hall bar. Despite of those progresses, detailed knowledge about the microscopic mechanisms of AHE in this kind of material remains a shortage and needs further exploration in the future.

4. Conclusion

Numerous studies have been carried out on the synthesis and characterizations of Mn_xGa and Mn_xAl epitaxial films with perpendicular magnetic anisotropy. Mn_xGa alloys with both $L1_0$ and $D0_{22}$ ordering show giant perpendicular magnetic anisotropy, high spin polarization, high Curie temperature, huge coercivity, moderate magnetization, large energy product, low damping constant, giant Kerr rotation, large anomalous Hall resistivity, and high thermal dynamical stability. $L1_0$-ordered Mn_xAl films grown on GaAs and MgO also exhibit giant perpendicular anisotropy, high Curie temperature, huge coercivity, moderate magnetization, large energy product, giant Kerr rotation, and large anomalous Hall resistivity. Importantly, the magnetism of both Mn_xGa and Mn_xAl films could be tailored effectively by several methods including controlling the growth temperature, tuning the composition, varying annealing conditions, and selecting different substrates. These pronounced magnetic properties and effective controllability make these perpendicularly magnetized Mn-based binary alloy films very promising for high-performance novel spintronic devices, ultrahigh-density perpendicular magnetic recording, and economical permanent magnets, although there have rarely been progresses on high-performance spintronic devices, magnetic recording, or practical permanent magnet applications. Moreover, the Mn_xGa and Mn_xAl ferromagnetic films with both high K_u and good compatibility with semiconductors have great applications not only in semiconductor spintronics like spin-LED, spin-FET, and lateral spin valves with perpendicular spin injectors and detectors, but also in the high-density integration of metallic spintronic functional devices like nonvolatile magneto-resistive random access memory on semiconductor photonic and electronic circuits.

References

[1] Chappert C, Fert A and Dau F N V 2007 *Nat. Mater.* **6** 813
[2] Ikeda S, Miura K, Yamamoto H, Mizunuma K, Gan H D, Endo M, Kanai S, Hayakawa J, Matsukura F and Ohno H 2010 *Nat. Mater.* **9** 721
[3] Mangin S, Ravelosona D, Katine J A, Carey M J, Terris B D and Fullerton E E 2006 *Nat. Mater.* **5** 210
[4] Houssameddine D, Ebels U, Delaët B, Rodmacq B, Firastrau I, Ponthenier F, Brunet M, Thirion C, Michel J P, Prejbeanu-Buda L, Cyrille M C, Redon O and Dieny B 2007 *Nat. Mater.* **6** 447
[5] Mancoff F B, Dunn J H, Clemens B M and White R L 2000 *Appl. Phys. Lett.* **77** 1879
[6] Datta S and Das B 1990 *Appl. Phys. Lett.* **56** 665
[7] Koo H C, Kwon J H, Eom J, Chang J, Han S H and Johnson M 2009 *Science* **325** 1515
[8] Wunderlich J, Park B, Irvine A C, Zârbo L P, Rozkotová E, Nemec P, Novák V, Sinova J and Jungwirth T 2010 *Science* **330** 1801
[9] Kohda M, Kita T, Ohno Y, Matsukura F and Ohno H 2006 *Appl. Phys. Lett.* **89** 012103
[10] Ohno Y, Young D K, Beschoten B, Matsukura F, Ohno H and Awschalom D D 1999 *Nature* **402** 790
[11] Lou X, Adelmann C, Crooker S A, Garlid E S, Zhang J J, Reddy K S M, Flexner S D, Palmstrøm C J and Crowell P A 2007 *Nat. Mater.* **3** 197
[12] Adelmann C, Hilton J L, Schultz B D, McKernan S, Palmstrøm C J, Lou X, Chiang H S and Crowell P A 2006 *Appl. Phys. Lett.* **89** 112511
[13] Lu E, Ingram D C, Smith A R, Knepper J W and Yang F Y 2006 *Phys. Rev. Lett.* **97** 146101
[14] Tanaka M, Harbison J P, DeBoeck J, Sands T, Philips B, Cheeks T L and Keramidas V G 1993 *Appl. Phys. Lett.* **62** 1565
[15] Krishnan K M 1992 *Appl. Phys. Lett.* **61** 2365
[16] Zhu L J, Nie S H, Meng K K, Pan D, Zhao J H and Zheng H Z 2012 *Adv. Mater.* **24** 4547
[17] Zhu L J, Pan D, Nie S H, Lu J and Zhao J H 2013 *Appl. Phys. Lett.* **102** 132403
[18] Ohno H 2010 *Nat. Mater.* **9** 952
[19] Challener W A, Peng C, Itagi A V, Karns D, Peng W, Peng Y G, Yang X M, Zhu X B, Gokemeijer N J, Hsia Y T, Ju G, Rottmayer R E, Seigler M A and Gage E C 2009 *Nat. Photon* **3** 220
[20] Gutfleisch O, Willard M A, Brück E, Chen C H, Sankar S G and Liu J P 2011 *Adv. Mater.* **23** 821
[21] Sakuma A 1998 *J. Magn. Magn. Mater.* **187** 105
[22] Mizukami S, Wu F, Sakuma A, Walowski J, Watanabe D, Kubota T, Zhang X, Naganuma H, Oogane M, Ando Y and Miyazaki T 2011 *Phys. Rev. Lett.* **106** 117201

[23] Yang Z, Li J, Wang D, Zhang K and Xie X 1998 *J. Magn. Magn. Mater.* **182** 369
[24] Zhu L J and Zhao J H 2013 *Appl. Phys. A* **111** 379
[25] Winterlik J, Balke B, Fecher G H, Felser C, Alves M C M and Bernardi F and Morais J 2008 *Phys. Rev. B* **77** 054406
[26] Nie S H, Zhu L J, Lu J, Pan D, Wang H L, Yu X Z, Xiao J X and Zhao J H 2013 *Appl. Phys. Lett* **102** 152405
[27] Sakuma A 1994 *J. Phys. Soc. Jpn.* **63** 1422
[28] Meissner H G and Schubert K 1965 *Z. Metallkd.* **56** 523
[29] Wu J S and Kuo K H 1997 *Metall. Mater. Trans. A* **28** 729
[30] Massalski T B 1990 *Binary Alloy Phase Diagrams* (2nd edn) (Materials Park: Materials Information Soc.)
[31] Bither T A and Cloud W H 1965 *J. Appl. Phys.* **36** 1501
[32] Lu X, Liang J and Yang Z 1979 *Acta Phys. Sin.* **28** 54 (in Chinese)
[33] Krén E and Kádár G 1970 *Solid State Commun.* **8** 1653
[34] Niida H, Hori T, Onodera H, Yamaguchi Y and Nakagawa Y 1996 *J. Appl. Phys.* **79** 5946
[35] Kurt H, Rode K, Venkatesan M, Stamenov P and Coey J M D 2011 *Phys. Status. Solidi B* **248** 2338
[36] Mizukami S, Kubota T, Wu F, Zhang X, Miyazaki T, Naganuma H, Oogane M, Sakuma A and Ando Y 2012 *Phys. Rev. B* **85** 014416
[37] Huh Y, Kharel P, Shah V R, Li X Z, Skomski R and Sellmyer D J 2013 *J. Appl. Phys.* **114** 013906
[38] Krishnan K M 1992 *Appl. Phys. Lett.* **61** 2365
[39] Tanaka M, Harbison J P, DeBoeck J, Sands T, Philips B, Cheeks T L and Keramidas V G 1993 *Appl. Phys. Lett.* **62** 1565
[40] Lu E, Ingram D C, Smith A R, Knepper J W and Yang F Y 2006 *Phys. Rev. Lett.* **97** 146101
[41] Bedoya-Pinto A, Zube C, Malindretos J, Urban A and Rizzi A 2011 *Phys. Rev. B* **84** 104424
[42] Wang K, Lu E, Knepper J W, Yang F and Smith A R 2011 *Appl. Phys. Lett.* **98** 162507
[43] Feng W, Thiet D V, Dung D D, Shin Y and Chob S 2010 *J. Appl. Phys.* **108** 113903
[44] Wang K, Chinchore A, Lin W, Ingram D C, Smith A R, Hauser A J and Yang F 2009 *J. Cry. Growth* **311** 2265
[45] Wu F, Sajitha E P, Mizukami S, Watanabe D, Miyazaki T, Naganuma H, Oogane M and Ando Y 2010 *Appl. Phys. Lett.* **96** 042505
[46] Wu F, Mizukami S, Watanable D, Naganuma H, Oogane M and Ando Y 2009 *Appl. Phys. Lett.* **94** 122503
[47] Kurt H, Rode K, Venkatesan M, Stamenov P and Coey J M D 2011 *Phys. Rev. B* **83** 020405
[48] Nummy T J, Bennett S P, Cardinal T and Heiman D 2011 *Appl. Phys. Lett.* **99** 252506
[49] Zha C L, Dumas R K, Lau J W, Mohseni S M, Sani S R, Golosovsky I V, Monsen Å F, Nogueś J and Åkerman J 2011 *J. Appl. Phys.* **110** 093902
[50] Kubota T, Araidai M, Mizukami S, Zhang X, Ma Q, Naganuma H, Oogane M, Ando Y, Tsukada M and Miyazaki T 2011 *Appl. Phys. Lett.* **99** 192509
[51] Kubota T, Mizukami S, Watanabe D, Wu F, Zhang X, Naganuma H, Oogane M, Ando Y and Miyazaki T 2011 *J. Appl. Phys.* **110** 013915
[52] Kubota T, Ma Q, Mizukami S, Zhang X, Naganuma H, Oogane M, Ando Y and Miyazaki T 2012 *Appl. Phys. Express* **5** 043003
[53] Ma Q L, Kubota T, Mizukami S, Zhang X M, Naganuma H, Oogane M, Ando Y and Miyazaki T 2012 *Appl. Phys. Lett.* **101** 032402
[54] Glas M, Imort I M, Thomas P, Reiss G and Ebke D 2013 *J. Magn. Magn. Mater.* **333** 134
[55] Brataas A, Kent A D and Ohno H 2012 *Nat. Mater.* **11** 372
[56] Yu J, Ruediger U, Kent A D, Farrow R F C, Marks R F, Weller D, Folks L and Parkin S S P 2000 *J. Appl. Phys.* **87** 6854
[57] He P, Ma L, Shi Z, Guo G Y, Zheng J G, Xin Y and Zhou S M 2012 *Phys. Rev. Lett.* **109** 066402
[58] Zhu L J, Pan D and Zhao J H *Proper Scaling of Anomalous Hall Effect in Disordered* $L1_0$-$Mn_{1.5}Ga$ (to be published)
[59] Hilton J L, Schultz B D, McKernan S and Palmstrøm C J 2004 *Appl. Phys. Lett.* **84** 3145
[60] Roy W V, Akinaga H, Miyanishi S, Tanaka K and Kuo L H 1996 *Appl. Phys. Lett.* **69** 711
[61] Wang K, Chinchore A, Lin W, Smith A and Sun K 2009 *MRS. Proceedings* **1118** 1118
[62] Bai Z, Cai Y, Shen L, Yang M, Ko V, Han G and Feng Y 2012 *Appl. Phys. Lett.* **100** 022408
[63] Zha C L, Dumas R K, Persson J, Mohseni S M, Nogueś J and Åkerman J 2010 *IEEE Mag. Lett.* **1** 2500104
[64] Roy W V, Akinaga H and Miyanishi S 2001 *Phys. Rev. B* **63** 184417
[65] Jiménez-Villacorta F, Marion J L, Sepehrifar T, Daniil M, Willard M A and Lewis L H 2012 *Appl. Phys. Lett* **100** 112408
[66] Koch A J J, Hokkeling P, Steeg M G and Vos K J 1960 *J. Appl. Phys.* **31** 75
[67] Ohtani T, Kato N, Kojima K, Sakamoto Y, Konno I, Tsukahara M and Kubo T 1997 *IEEE Trans. Magn.* **13** 1328
[68] Sands T, Harbison J P, Leadbeater M L, Allen S J, Hull G W, Ramesh R, Florez L T and Keramidas V G 1990 *Appl. Phys. Lett* **57** 2609
[69] Leadbeater M L, Allen S J, DeRosa F, Harbison J P, Sands T, Ramesh R, Florez L T and Keramidas V G 1991 *J. Appl. Phys.* **69** 4689
[70] Nie S H, Zhu L J, Pan D, Lu J and Zhao J H 2013 *Acta Phys. Sin.* **62** 178103 (in Chinese)
[71] Cheeks T L, Brasil M J S P, Sands T, Harbison J P, Aspnes D E, Keramidas V G and Allen S J 1992 *Appl. Phys. Lett* **60** 1393
[72] Boeck J D, Sands T, Harbison J P, Scherer A, Gilchrist H, Cheeks T L, Tanaka M and Keramidas V G 1993 *Electron. Lett.* **29** 421
[73] Roy W V, Boeck J D, Bender H, Bruynseraede C, Esch A V and Borghs G 1995 *J. Appl. Phys.* **78** 398
[74] Rosier T M, He Y W and El-Masry N A 1996 *Mater. Lett.* **26** 227
[75] Saruyama H, Oogane M, Kurimoto Y, Naganuma H and Ando Y 2013 *Jpn. J. Appl. Phys.* **52** 063003
[76] Hosoda M, Oogane M, Kubota M, Kubota T, Saruyama H, Lihama S, Naganuma H and Ando Y 2012 *J. Appl. Phys.* **111** 07A324
[77] Angadi M A and Thanigaimani V 1991 *Thin Solid Films* **195** 7
[78] Zhang D, Xu X, Wang W, Zhang X, Yang H, Wu Y, Ma C and Jiang Y 2012 *Rare Metals* **31** 112